particles

IMPACT FACTOR 1.7

CITESCORE 3.2

Article

Black Hole's Spin-Dependence of γ-Ray and Neutrino Emissions from MAXI J1820+070, XTE J1550-564, and XTE J1859+226

Dimitrios Rarras, Odysseas Kosmas, Theodora Papavasileiou and Theocharis Kosmas

Special Issue

Testing Fundamental QED and BSM Physics Theories in Leptonic and Hadronic Processes

Edited by

Prof. Dr. Theocharis Kosmas, Prof. Dr. Hiroyasu Ejiri and Prof. Dr. John Vergados

MDPI

https://doi.org/10.3390/particles7030049

particles

MDPI

Article

Black Hole's Spin-Dependence of γ-Ray and Neutrino Emissions from MAXI J1820+070, XTE J1550-564, and XTE J1859+226

Dimitrios Rarras [1,†], Odysseas Kosmas [1,*,†,‡], Theodora Papavasileiou [1,2,†] and Theocharis Kosmas [1,†]

[1] Department of Physics, University of Ioannina, GR-45110 Ioannina, Greece; rarrasdimitrios@gmail.com (D.R.); th.papavasileiou@uowm.gr (T.P.); hkosmas@uoi.gr (T.K.)
[2] Department of Informatics, University of Western Macedonia, GR-52100 Kastoria, Greece
* Correspondence: odykosm@gmail.com
† These authors contributed equally to this work.
‡ Current address: Conigital Ltd., 51 Parkside, Coventry CV1 2HG, UK.

Abstract: A black hole's spin effects on the jet emissions of high-energy neutrinos and γ-rays from black hole X-ray binary systems (BHXRBs) are investigated. The BHXRBs consist of a stellar black hole, a companion (donor) star, a BH accretion disk, a BH corona, and two jets emitted from the black hole perpendicular to the accretion disk. For their description, properties of the accretion disk, specifically the accretion disk's inner radius R_{in} and the accretion disk's temperature profile $T(R)$, play key roles since they depend on the black hole's dimensionless spin parameter α_*. In this work, we focus on the main reaction mechanisms taking place inside jets from which high-energy γ-rays and neutrinos are created. The intensities and integral fluxes of neutrinos and γ-rays are obtained by integrating the respective source functions. Lastly, the γ-ray absorption due to e^--e^+ pair production is considered, particularly absorption from the accretion disk. For concrete applications, we have chosen the BHXRB systems MAXI J1820+070, XTE J1550-564, and XTE J1859+226.

Keywords: stellar black holes; Kerr black holes; black hole X-ray binaries; jet emissions; gamma-ray absorption; neutrino emission intensities; gamma-ray emission fluxes; black hole spin effects

check for updates

Citation: Rarras, D.; Kosmas, O.; Papavasileiou, T.; Kosmas, T. Black Hole's Spin-Dependence of γ-Ray and Neutrino Emissions from MAXI J1820+070, XTE J1550-564, and XTE J1859+226. *Particles* **2024**, *7*, 818–833. https://doi.org/10.3390/particles7030049

Academic Editor: Manuela Vecchi

Received: 29 July 2024
Revised: 6 September 2024
Accepted: 10 September 2024
Published: 12 September 2024

Copyright: © 2024 by the authors. Licensee MDPI, Basel, Switzerland. This article is an open access article distributed under the terms and conditions of the Creative Commons Attribution (CC BY) license (https://creativecommons.org/licenses/by/4.0/).

1. Introduction

In recent years, multi-messenger emissions from black holes have attracted the intense interest of researchers dealing with galactic and extragalactic structures [1,2]. Among them, gamma rays and neutrinos possess prominent positions because appreciably sensitive ground-based and space-based telescopes are in operation or have been designed to operate in the near future [3–5].

In general, there are two classes of multi-messenger emission sources distinguished by the scale and energy-emission range. In the class of extragalactic sources, active galactic nuclei (AGN) with a supermassive black hole at their center emit extremely high-energy gamma-rays, neutrinos, etc. [6,7], while Galactic sources usually emit gamma-rays, neutrinos, X-rays, radio waves, etc., which are in the observation spectrum of operating telescopes [8,9].

Our interest in the present work is focusing on high-energy gamma-ray and neutrino jet-emissions emanating from rotating (Kerr) black holes, specifically those of galactic stellar black hole X-ray binaries (BHXRBs). Among the relevant sources, MAXI J1820+070 [10,11], XTE J1550-564 [12,13], and XTE J1859+226 [14,15] are included, in which spin has been recently observed. Rotating stellar black holes (Kerr BHs) are characterized by their spin, which, in the above systems, covers a rather wide range. The most important parameter entering the description of the above emissions is the black hole's dimensionless spin parameter α_*.

We specifically calculate high-energy gamma-ray and neutrino intensities and fluxes within the context of the lepto-hadronic jet model. This model starts from the fundamental

reaction mechanisms that lead to the production of high-energy gamma-rays and neutrinos [16–18]. In the calculations performed up to now, we have not taken into account the black hole's spin; however, in the systems mentioned above, the spin may significantly affect the emitted gamma-ray spectra due to various absorption mechanisms [19–22], among which the most significant are absorptions due to the accretion disk, the black hole corona, and the donor star's wind. In the case of the accretion disk, the key role is played by the inner radius (R_{in}) of the disk, which is located at the radius of the innermost stable circular orbit (R_{ISCO}), see, e.g., [23,24], and the disk's temperature profile [25,26].

The remainder of the article is structured as follows. In Section 2, the accretion disk's properties are summarized, stressing the accretion disk's inner radius and its temperature profile. Next, in Section 3, the main reaction mechanisms inside the jets are presented, and the transfer equation, which describes the energy distribution of each kind of particle, is also included. The calculations of the expected intensities and integral fluxes are explained in Section 4, as well as the absorption effects on the gamma-rays. In Section 5, the three BHXRB systems studied in this work, i.e., MAXI J1820+070, XTE J1550-564, and XTE J1859+226, are presented by concentrating on their main properties. Detailed results of high-energy neutrino and gamma-ray intensities, as well as the corresponding fluxes, are discussed for each system. In Section 6, a technique of measuring the black hole's spin α_* in BHXRBs that came out of our present investigation is proposed. Lastly, in Section 7, we summarize the main conclusions extracted from the present work and discuss future prospects.

2. Spin-Induced Modifications of the Accretion Disk's Properties

In this section, we will discuss two main properties of the accretion disk necessary for our analysis: the accretion disk's inner radius and temperature profile.

2.1. Inner Radius of the Accretion Disk around a Kerr Black Hole

A crucial parameter usually employed to treat the physics around Kerr black holes is the radius attributed to the innermost circular stable orbits, R_{ISCO}, of particles around the black hole on its equatorial plane. It is given by the following expression [24]:

$$R_{ISCO} = r_g\{3 + Z_2 \mp [(3 - Z_1)(3 + Z_1 + 2Z_2)]^{1/2}\}, \quad (1)$$

where

$$Z_1 \equiv 1 + \left(1 - \alpha_*^2\right)^{1/3}\left[(1 + \alpha_*)^{1/3} + (1 - \alpha_*)^{1/3}\right],$$
$$Z_2 \equiv \left(3\alpha_*^2 + Z_1^2\right)^{1/2}.$$

The gravitational radius is $r_g = \frac{GM_{BH}}{c^2}$, with M_{BH} of the mass the black hole. In Equation (1), the minus $(-)$ sign corresponds to the co-rotating case of the particle and the black hole, while the plus $(+)$ sign corresponds to the counter-rotating case.

This radius greatly depends on the spin of the black hole, which is represented by the dimensionless spin parameter $\alpha_* = \frac{cJ}{GM_{BH}^2}$, where J is the angular momentum of the black hole. In the limit $\alpha_* = 0$, we recover $R_{ISCO} = 6r_g$ corresponding to the Schwarzschild case, while the extreme Kerr limit $\alpha_* = 1$ yields $R_{ISCO} = r_g$ for the co-rotation case (i.e., between the accretion flow and the black hole), and $R_{ISCO} = 9r_g$ for the counter-rotating orbits. This radial limit plays a crucial role when accounting for the absorption induced by the accretion disk, as it is assumed to replicate its respective innermost boundary as follows:

$$R_{in} = R_{ISCO}. \quad (2)$$

2.2. Disk Temperature Profile Derived from the Pseudo-Newtonian Potential

Acquiring the disk temperature profile requires the angular velocity of the disk, which is defined as follows [25]:

$$\omega_{disk} = \left(\frac{1}{r}\frac{d\Phi}{dr}\right)^{1/2}, \tag{3}$$

where Φ denotes the gravitational potential. Then, the emitted luminosity of the disk per surface area is calculated as follows:

$$F_{disk} = \frac{-\dot{M}(j - j_0)}{4\pi r}\frac{d\omega_{disk}}{dr}, \tag{4}$$

where $\dot{M}$ is the accretion rate at which mass from the donor star accumulates to the equatorial region of the black hole in a binary system, $j = \omega_{disk} r^2$ is the specific angular momentum of the disk at radius r, and j_0 is the specific angular momentum of the disk at R_{in}. Finally, the radial temperature emerges from the Stefan-iBoltzmann law as follows:

$$T(r) = \left(\frac{F_{disk}}{\sigma_{SB}}\right)^{1/4}, \tag{5}$$

where σ_{SB} is the Stefan–Boltzmann constant.

Integration of the black hole's rotation urges the need for an appropriate gravitational potential. In this work, we employ the potential proposed by Mukhopadhyay in [26]. It is derived directly from the Kerr metric that yields a centrifugal force, given per mass units, as follows:

$$F = \frac{c^2}{r_g}\frac{\left(\bar{r}^2 - 2a_*\sqrt{\bar{r}} + a_*^2\right)}{\bar{r}^3\left(\sqrt{\bar{r}}(\bar{r} - 2) + a_*\right)^2}. \tag{6}$$

The radius is written in units of the gravitational radius as $\bar{r} = r/r_g$. The analytical form of the potential is algebraically complicated and, thus, replaced with the numerical integration of the below expression:

$$\Phi = -\int_{R_{in}}^{R_\infty} F dr. \tag{7}$$

For the extraction of this pseudo-Newtonian potential, the general relativity formalism concerning the Kerr geometry is implemented. It works for every value of α_*, including the negative spin values corresponding to the retrograde case, and retains a maximum error of 10% regarding the occurring energy dissipation distribution and the mechanical energy at R_{ISCO}.

Using Equations (3)–(5) and (7), we obtain the spin-dependent temperature profile of the accretion disk as follows [27]:

$$T(r) = T_o\left(\frac{4\mathcal{R}(\bar{r})^2}{3\bar{r}^4} - \mathcal{L}(\bar{r})\right)^{1/4}\left(1 - \frac{\mathcal{R}(\bar{r}_{in})}{\mathcal{R}(\bar{r})}\right)^{1/4}, \tag{8}$$

where we have define the following functions:

$$\mathcal{R}(\bar{r}) = \frac{\bar{r}^2 - 2\alpha_*\sqrt{\bar{r}} + \alpha_*^2}{\sqrt{\bar{r}}(\bar{r} - 2) + \alpha_*},$$
$$\mathcal{L}(\bar{r}) = \frac{2\mathcal{R}(\bar{r})}{3\bar{r}^3\left(\sqrt{\bar{r}}(\bar{r} - 2) + \alpha_*\right)}\left(2\bar{r} - \frac{\alpha_*}{\sqrt{\bar{r}}} - \frac{3\bar{r} - 2}{2\sqrt{\bar{r}}}\mathcal{R}(\bar{r})\right).$$

Furthermore, the dependence on the black hole's mass and the accretion rate is sustained through the following constant:

$$T_o = \left(\frac{3GM_{BH}\dot{M}}{8\pi\sigma_{SB}r_g^3}\right)^{1/4}.$$

In most BHXRBs, the total luminosity radiated away from the disk does not exceed the Eddington limit $L_{disk} \approx 10^{38}\text{ergs}^{-1}$, corresponding to an accretion rate of approximately $\dot{M}_{accr} \approx 10^{-8} M_{\odot}\text{yr}^{-1}$, which we adopt in our study. The temperature associated with the innermost stable orbit falls in the range of $T \sim 10^6 - 10^7$ K. Note that the higher the value of a_*, the higher the temperature, while negative values of a_* (retrograde case) lead to gradually decreasing temperatures.

3. The Relativistic Jets in BHXRBs

3.1. Reaction Chains within the Relativistic Jets

Concerning the BHXRB sources, two jets propagate away from the black hole perpendicularly to the accretion disk's plane. Its content consists of plasma of a lepto-hadronic nature. In this work, we adopt the value $a_k = L_p/L_e = 10^{-2}$ for the jet's hadron-to-lepton ratio, where L_p (L_e) stands for the proton (electron) kinetic luminosity. Moreover, a small portion of the particles, $q_r = 10^{-4}$, assumes relativistic energies via shock-wave propagation within a slice of the jet from $z_0 = 10^9$ cm to $z_{max} = 5z_0$. A vital model parameter determining the efficiency with which the jet particles are being accelerated is $\eta = L_k/L_{input} = 0.1$, which describes the percentage of the total input luminosity, L_{input} (from the magnetic field and the accretion disk), which is converted to the kinetic luminosity, L_k, of the particles moving inside the jet.

Two main chain reactions occur inside the jet, leading to high-energy gamma-rays and neutrinos. Specifically, the relativistic protons interact with the cold hadronic matter of the jet, as well as with photons originating from internal and external emission sources, see [28–30]. The first chain reaction begins with proton–proton, $p-p$, collisions as follows:

$$\begin{aligned} pp &\longrightarrow pp + a\pi^0 + \beta\pi^+\pi^-, \\ pp &\longrightarrow pn + \pi^+ + a\pi^0 + \beta\pi^+\pi^-, \\ pp &\longrightarrow nn + 2\pi^+ + a\pi^0 + \beta\pi^+\pi^-, \end{aligned} \tag{9}$$

where a and β are multiplicities depending on the proton energy E_p ($a, \beta \sim E_p^{-1/4}$), see [31]. The second chain of reactions is triggered by proton–photon, $p-\gamma$, scatterings:

$$\begin{aligned} p\gamma &\longrightarrow n\pi^+, \\ p\gamma &\longrightarrow p\pi^0, \\ p\gamma &\longrightarrow p\pi^0\pi^+\pi^-. \end{aligned} \tag{10}$$

Subsequently, the neutral pions decay to gamma-ray photons as follows:

$$\pi^0 \longrightarrow \gamma + \gamma, \tag{11}$$

while the charged pions decay to muons and muon neutrinos. The muons (or antimuons) decay to electrons (or positrons) and electron neutrinos (or antineutrinos).

$$\begin{aligned} \pi^+ &\longrightarrow \mu^+\nu_\mu \longrightarrow e^+\bar{\nu}_\mu\nu_e + \nu_\mu, \\ \pi^- &\longrightarrow \mu^-\bar{\nu}_\mu \longrightarrow e^-\nu_\mu\bar{\nu}_e + \bar{\nu}_\mu. \end{aligned} \tag{12}$$

3.2. Solution of the Transfer Equation

The governing equation that describes the evolution of the particle energy distributions inside the jet is the transfer equation, whose general form can be found in [32]. However, in this work, we will use an appropriate approximation for astrophysical jets, the steady-state transfer equation, see [16,33,34]:

$$\frac{\partial N(E,z)b(E,z)}{\partial E} + t^{-1}N(E,z) = Q(E,z), \tag{13}$$

where its solution $N(E,z)$ is the energy distribution of each kind of particle inside the jet. $Q(E,z)$ is the particle source function, providing the respective production rate. $b(E)$ is the energy loss rate, which has the form $b(E) = dE/dt = -Et_{loss}^{-1}$, with t_{loss}^{-1} being the rate at which the particles lose energy. The rate t^{-1} is given as the sum $t^{-1} = t_{esc}^{-1} + t_{dec}^{-1}$, with $t_{esc}^{-1} = c/(z_{max} - z_0)$ being the rate of the particles escaping the acceleration zone and t_{dec}^{-1} their decay rate.

The solution of the transfer equation is as follows (see [35–39]):

$$N(E,z) = \frac{1}{|b(E)|}\int_E^{E_{max}} Q(E',z)e^{-\tau(E,E')}dE', \tag{14}$$

where

$$\tau(E,E') = \int_E^{E'} \frac{t^{-1}}{|b(E'')|}dE''. \tag{15}$$

It should be noted that the above integration is conducted numerically. Moreover, each particle species involved in the chain reactions of Equations (9)–(12) is treated differently within the context of the transfer equation. The emerging particle distributions retain the parent particle's spectral shape through their source function $Q_j(E,z)$, which provides the production rate yielded from the respective interaction cross-sections [17,18]. After solving the occurring set of coupled equations and obtaining the respective energy distributions, we compute the source functions of high-energy neutrinos Q_ν and gamma-rays Q_γ, which is the focal point of our research.

In recent research, a more general form of the transfer equation, with more terms taken into account, is being used [40,41]:

$$\frac{\partial N(E,t,z)}{\partial t} + \frac{\partial(\Gamma(t,z)v(t,z)N(E,t,z))}{\partial z} + \frac{\partial N(E,t,z)b(E,t,z)}{\partial E} + t^{-1}N(E,t,z) = Q(E,t,z). \tag{16}$$

In the transfer equation of Equation (16), the first term represents the temporal evolution of the energy distribution, while the second term represents the propagation of particles along the jet, where $\Gamma(t,z)$ and $v(t,z)$ are the Lorentz factor along the jet and its bulk velocity, respectively. Calculations including contributions from such terms of the transfer equation will be included in future works.

4. High-Energy Gamma-Ray and Neutrino Emissions

4.1. Intensities and Integral Fluxes

If we integrate the source functions of the neutrinos and gamma-rays over the acceleration zone, we obtain the respective intensities [38,39]:

$$I_\nu(E_\nu) = \int_V Q_\nu(E_\nu,z)d^3r = \pi\tan^2\xi\int_{z_0}^{z_{max}} Q_\nu(E_\nu,z)z^2dz, \tag{17}$$

and

$$I_{\gamma,o}(E_\gamma) = \int_V Q_\gamma(E_\gamma,z)d^3r = \pi\tan^2\xi\int_{z_0}^{z_{max}} Q_\gamma(E_\gamma,z)z^2dz, \tag{18}$$

where the right-hand sides account for the conical geometry of the jet. However, a part of the γ-rays emitted from the jet can be absorbed due to photon annihilation, which leads to $e^+ - e^-$ production as follows:

$$\gamma + \gamma \longrightarrow e^+ + e^-. \tag{19}$$

This can happen if a γ-ray emitted from the jet interacts with a lower energy photon from the accretion disk, the donor star, or the corona. This leads to the corresponding attenuations $\mathcal{A}_{disk}$, $\mathcal{A}_{donor}$ and $\mathcal{A}_{cor}$, which depend on various parameters of the binary

system and represent the rate at which the γ-rays are being annihilated. As a result, their initial intensity $I_{\gamma,0}$ will be reduced to the following:

$$I_\gamma = I_{\gamma,o} e^{-\mathcal{A}_{all}}, \tag{20}$$

where $\mathcal{A}_{all}$ is the sum of the attenuations corresponding to all the varying photo-absorption sources.

The corresponding integral fluxes emitted are calculated as follows:

$$\Phi_j = \int_{E_{min}}^{E_{max}} \frac{I_j(E_j) dE_j}{4\pi d^2}, \tag{21}$$

where $E_{min} = 10^2\ GeV$ and $j = \nu, \gamma$ for neutrinos and gamma-rays, respectively.

4.2. Absorption from the Accretion Disk

In this subsection, we will discuss the photon absorption due to the interaction described by Equation (19). The accretion disk consists of overheated matter and gas rotating around the system's black hole. We will focus on the disk-induced attenuation, $\mathcal{A}_{disk}$, as it is the dominant one near the ejected plasma while still tightly collimated. In this jet-propagation stage, $\mathcal{A}_{disk}$ attains some orders of magnitudes more than the ones corresponding to the donor star, $\mathcal{A}_{donor}$, and especially from the corona, $\mathcal{A}_{cor}$.

Due to the presence of the magnetic field and high temperature, the disk emits soft X-ray photons capable of absorbing jet gamma-ray photons when they collide with an angle θ_0. The cross-section of this interaction is as follows [19]:

$$\sigma_{\gamma\gamma}(E_\gamma, \epsilon, \theta_0) = \frac{\pi e^4}{2m_e^2 c^4}(1-\beta^2)\left[(3-\beta^4)\ln\left(\frac{1+\beta}{1-\beta}\right) - 2\beta(2-\beta^2)\right], \tag{22}$$

where ϵ is the energy of the less-energetic photon originating from the accretion disk. In above expression, the following holds:

$$\beta = \sqrt{1-\frac{1}{s}}, \qquad s = \frac{\epsilon E_\gamma (1-\cos\theta_0)}{2m_e^2 c^4},$$

where, for a pair to occur, it needs to be $s > 1$.

The disk attenuation $\mathcal{A}_{disk}$ is provided by integrating the X-ray photon energy, the distance that the high-energy photons travel from the emission source to the observer l, and the disk's radius R and angle ϕ as [20]:

$$\mathcal{A}_{disk} = \int_0^\infty \int_0^{2\pi} \int_{R_{in}}^{R_{out}} \int_{\epsilon_{min}}^\infty \frac{dn}{d\epsilon d\Omega}(1-\cos\theta_0)\sigma_{\gamma\gamma}\frac{\rho\cos\omega}{D^3} R d\epsilon dR d\phi dl. \tag{23}$$

Here, for $\epsilon_{min} = 2m_e^2c^4/E_\gamma(1-\cos\theta_0)$, ρ is the collision point's distance to the central object, D is the distance between the disk's surface element and the collision point, and ω is the angle between ρ and the z-axis. Analytically, the above quantities are provided as follows:

$$\rho = \left(z^2 + l^2 + 2lz\cos i\right)^{1/2}, \qquad D = \left(R^2 + \rho^2 - 2R\rho\cos\psi\right)^{1/2},$$
$$\psi = \cos^{-1}\left(\frac{l\sin i\cos\phi}{\rho}\right), \qquad \omega = \cos^{-1}\left(\frac{z + l\cos i}{\rho}\right),$$

where ψ is the angle between ρ and R, and i is the inclination angle of the jet's axis to the observer's line of sight.

If we assume thermal equilibrium between the infinitesimal surface elements of the disk, the emitted photon density follows the black-body radiation spectrum as follows:

$$\frac{dn}{d\epsilon d\Omega} = \frac{2}{h^2c^3}\frac{\epsilon^2}{e^{\mathcal{T}(R)}-1}, \tag{24}$$

where $\mathcal{T}(R) = \epsilon/k_B T(R)$, with k_B being the Boltzmann constant and h the Planck constant. As we have already mentioned, the disk begins at $R_{in} = R_{ISCO}$, with R_{ISCO} provided by Equation (1). For the temperature of the disk $T(R)$, we will use the temperature profile of Equation (8). Since the $\mathcal{A}_{disk}$ is a function of the R_{ISCO} and $T(R)$, it greatly depends on the dimensionless spin parameter a_*, which integrates the effects of the black hole's rotation on the jet emissions. A sketch of the attenuation process from the accretion disk is shown in Figure 1.

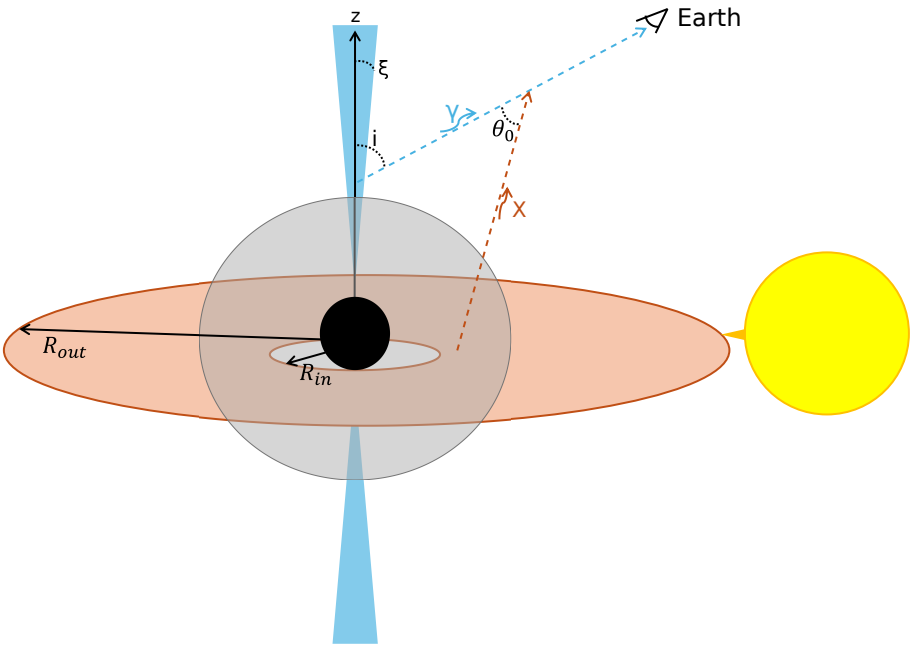

Figure 1. Sketch of a BHXRB and the attenuation of the jet's γ-rays from the accretion disk's X-rays. The black hole is in the center in black. The two oppositely directed jets are along the z axis in blue. The accretion disk is on the equatorial plane in brown. The donor star is on the right-hand side in yellow, while the Corona is in the center, around the black hole, in gray.

In addition to the absorption mechanisms integrated above, there are other radiation mechanisms, such as synchrotron self-compton (SSC) [42] and inverse compton (IC) scattering [43] from various regions of the BHXRB system, which could have an important influence on high-energy γ-ray emissions. Such effects will be included in our future works.

5. Results and Discussion

For the application of the lepto-hadronic model, we have selected a set of three BHXRB systems. Namely, they are the systems MAXI J1820+070, XTE J1550-564, and XTE J1859+226. We have selected these systems since they have different spin parameters, while their other parameters are similar. Thus, we can investigate how changing the spin of the system will change the results. Note that for most of them, there are three values for the spin parameter, with contradicting values between them, since there are three distinct methods to calculate the spin, namely the continuum fitting method (CFM) [44], the X-ray reflection spectroscopy method (XRS) [45], and the relativistic precession model (RPM) [46].

5.1. MAXI J1820+070

MAXI J1820+070 is a BHXRB candidate that is located at a distance $d = 2.96$ kpc from Earth. Its donor star is considered to be a subgiant of the K-type [47] with an effective temperature of $T_d = 4200$ K. Using a Hertzsprung–Russell diagram, we find

that its luminosity is $L_{star} = 7L_{\odot}$ [48]. The jet's bulk velocity is $u_b = 0.89c$. The jet half-opening angle is found to be $\xi = 1.5^{\circ}$. Regarding the spin of the black hole, the CFM provides $\alpha_* = 0.14 \pm 0.09$ (1σ) [49], the XRS is $\alpha_* = 0.988^{+0.006}_{-0.028}$ (1σ) [50], and the RPM is $\alpha_* = 0.799^{+0.016}_{-0.015}$ (1σ) [51], so we have to investigate all of them. It is worth mentioning that in systems for which the spin–orbit misalignment is rather large, the axis of the spin of the black hole is different than the orbital axis, and the system's geometry is different than the assumed above. Such an effect may appear in the MAXI J1820+070 system [52]. This means that the result obtained for the gamma-ray absorption of Section 4.2 should be modified [53]. The parameters of MAXI J1820+070 that we are going to use are depicted in Table 1.

Table 1. Main parameters of the MAXI J1820+070 system.

MAXI J1820+070				
$M_{BH}(M_{\odot})$	$M_{donor}(M_{\odot})$	d (kpc)	i (°)	P_{orb} (days)
8.48 [54]	0.49 [47]	2.96 [55]	63 [55]	0.68549 [52]
$L_{star}(L_{\odot})$	T_{eff} (K)	$u_b(c)$	ξ (°)	$a_* = \alpha/\mu$
7	4200 [47]	0.89 [55]	1.5 [56]	0.14/0.988/0.799

Figure 2a depicts the proton distribution. The dimensionless spin parameter α_* has no effect on the proton distribution since it does not appear in any of the equations of the protons. In Figure 2b, we see the intensity of neutrinos produced by pion decay, in which pions are produced by p–p reactions. The neutrino intensity remains the same for every value of α_*. The dimensionless spin parameter α_* has no effect on the intensity of neutrinos since it does not appear in the equations for neutrino production and since the neutrinos are not absorbed. The integral flux of neutrinos is $\Phi_{\nu} = 3.911684 \times 10^{-16} \nu \mathrm{cm}^{-2}\mathrm{s}^{-1}$.

Figure 2c depicts the attenuation of the accretion disk, $\mathcal{A}_{disk}$, for the three values of the dimensionless spin parameter α_*. For $\alpha_* = 0.14$, we have the lowest attenuation, which is significant in a narrower energy range, with the lowest maximum value. For $\alpha_* = 0.799$, we have higher attenuation, with a wider energy range and a larger maximum value. For $\alpha_* = 0.988$, we have the largest attenuation, with the widest energy range and the largest maximum. What we conclude is that the higher the α_*, the higher the attenuation of the accretion disk, with its range starting even earlier and with a larger maximum value at a lower energy. This can attributed to two factors. First, when α_* is increased, the R_{ISCO} becomes smaller, so the accretion disk has a larger surface from which a larger number of photons are emitted, which can annihilate a larger number of gamma-rays. The second factor is that when α_* is increased, the temperature profile of the disk increases as well, which leads to a larger black-body spectrum with a larger energy range and a larger peak at a smaller value of the energy. We can even see from the graph that the attenuation has similar behavior to a black-body spectrum, where the role of the temperature of the black-body spectrum plays the dimensionless spin parameter α_* for the attenuation.

In Figure 2d, we see the intensity of high-energy gamma-rays. The dashed black line represents the intensity without absorption, which is the same for every value of α_*, while the solid colored lines represent the intensity after absorption for the three values of α_*. For the case of absorption, the effect of the attenuation of the accretion disk for the three values α_* is obvious. Larger α_* means more absorption and, thus, a lower intensity. Finally, we examine the integral fluxes of high-energy gamma-rays for the three values of α_*. For $\alpha_* = 0.14$, we have $\Phi_{\gamma} = 8.668649 \times 10^{-13} \gamma \mathrm{cm}^{-2}\mathrm{s}^{-1}$. For $\alpha_* = 0.799$, we have $\Phi_{\gamma} = 7.925808 \times 10^{-13} \gamma \mathrm{cm}^{-2}\mathrm{s}^{-1}$. For $\alpha_* = 0.988$, we have $\Phi_{\gamma} = 6.617930 \times 10^{-13} \gamma \mathrm{cm}^{-2}\mathrm{s}^{-1}$. We observe that by increasing α_*, the integral flux decreases.

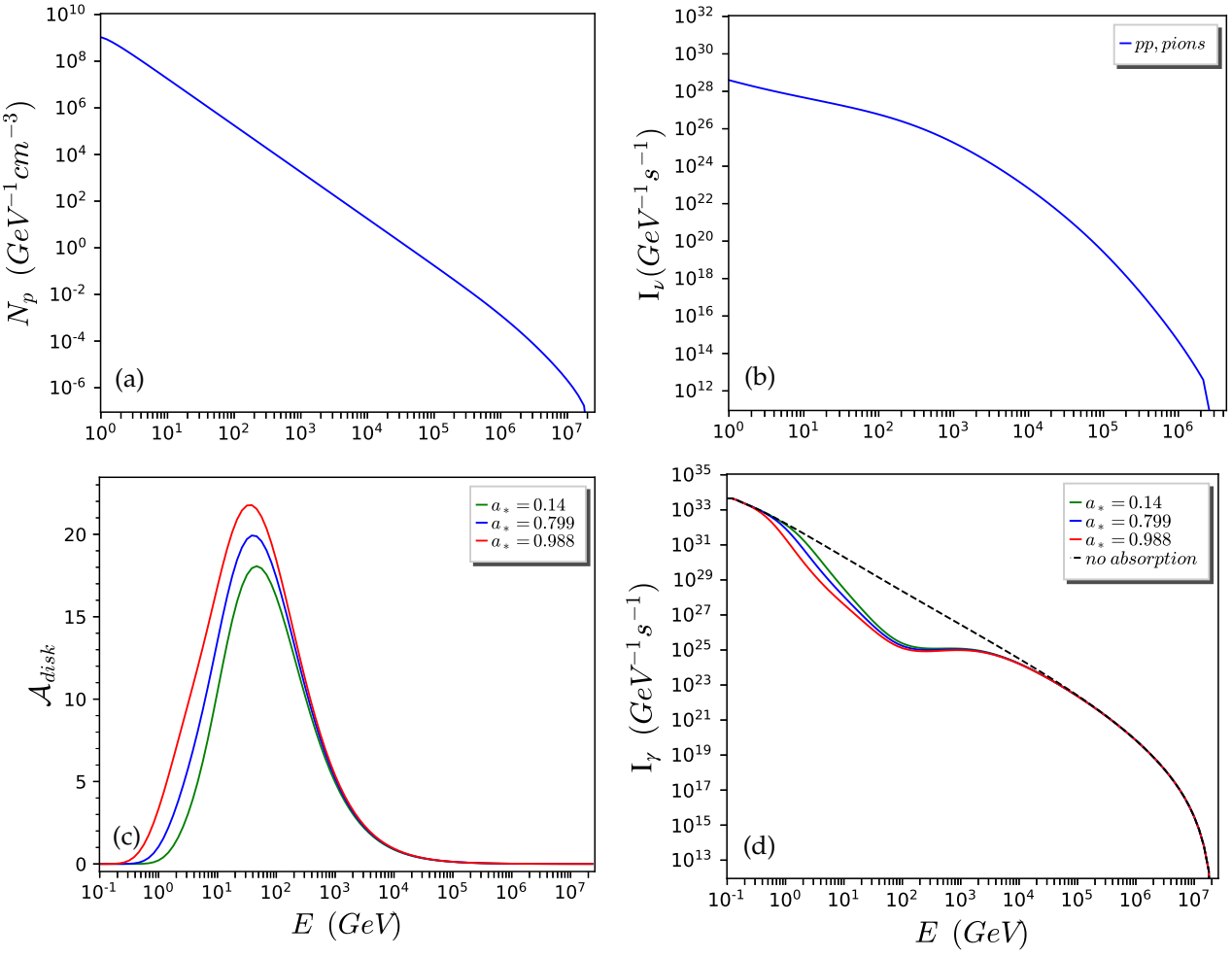

Figure 2. Results for MAXI J1820+070: (**a**) proton distribution (N_p), (**b**) intensity of neutrinos (I_ν) by pion decay produced by p–p reactions, (**c**) accretion disk's attenuation ($\mathcal{A}_{disk}$), and (**d**) intensity of high-energy γ-rays (I_γ).

5.2. XTE J1550-564

XTE J1550-564 is a BHXRB candidate that is located at a distance $d = 4.38$ kpc from Earth. Regarding the type of donor star, it is not exactly determined. It is believed to be either a K3-type main sequence star or a giant [57]. We will adopt that it is a main sequence star as its luminosity will be closer to the other systems. For a K3-type main sequence star, we determine that its effective temperature is $T_d = 4700$ K, and from a Hertzsprung–Russell diagram, we obtain that its luminosity is $L_{star} = 0.1 L_\odot$ [48]. The jet's Lorentz factor is $\Gamma_b = 19.6$ [58], from which we obtain a bulk velocity of $u_b = 0.99c$. The jet half-opening angle is found to be $\xi \leq 1^\circ$ [59], so we will use the value $\xi = 1^\circ$. The spin of the black hole is found using the CFM: $-0.11 < \alpha_* < 0.71$ at a $CL = 90\%$, with a most likely spin of $\alpha_* = 0.34$ [60]; the XRS: constrains it to be in the window of $0.33 < \alpha_* < 0.70$ at a $CL = 90\%$ with the best estimate at $\alpha_* = 0.55$ [60]; the RPM: $\alpha_* = 0.34 \pm 1$ (1σ) [61]. Steiner et al. combined the first two values to determine the synthesized result $0.29 < \alpha_* < 0.62$, with a most probable value of $\alpha_* = 0.49$ [60]. This is the value that we will adopt. The parameters that we will use for XTE J1550-564 are depicted in Table 2.

Table 2. Main parameters of the BHXRB system XTE J1550-564.

XTE J1550-564				
$M_{BH}(M_\odot)$	$M_{donor}(M_\odot)$	d (kpc)	i (°)	P_{orb} (days)
9.10 [57]	0.30 [57]	4.38 [57]	74.7 [57]	1.5420333 [57]
$L_{star}(L_\odot)$	T_{eff} (K)	$u_b(c)$	ξ (°)	a_*
0.1	4700 [57]	0.99	1	0.49

Figure 3a depicts the proton distribution. It has lower values than the proton distribution of MAXI J1820+070 because the inclination of this system is larger. In Figure 3b, we see the intensity of neutrinos. Again, lower values than that of MAXI J1820+070 are due to the larger inclination. The integral flux of neutrinos is $\Phi_\nu = 8.972519 \times 10^{-18} \nu \mathrm{cm}^{-2}\mathrm{s}^{-1}$. It is much lower than that of MAXI J1820+070 because of the larger inclination and the greater distance from Earth.

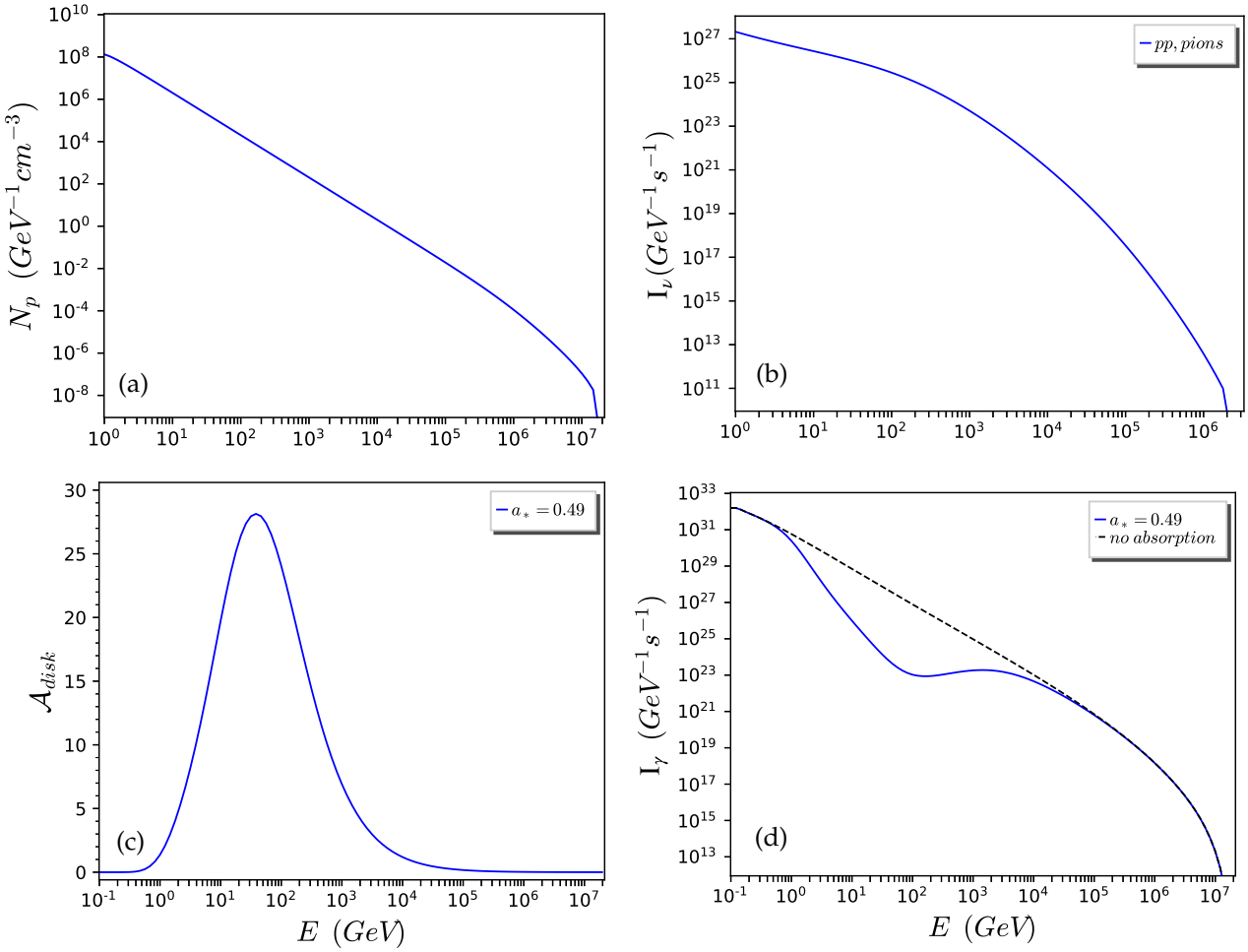

Figure 3. Results for XTE J1550-564: (**a**) proton distribution (N_p), (**b**) intensity of neutrinos (I_ν) by pion decay produced by p–p reactions, (**c**) accretion disk's attenuation ($\mathcal{A}_{disk}$), and (**d**) intensity of high-energy γ-rays (I_γ).

The attenuation of the accretion disk is depicted in Figure 3c. The attenuation is larger than MAXI J1820+070 even for its case of $a_* = 0.988$. This is because XTE J1550-564 has a larger inclination.

In Figure 3d, we see the intensity of gamma-rays. The intensity of high-energy gamma-rays is lower than that of MAXI J1820+070 due to the larger inclination of XTE J1550-564.

The integral flux of high-energy gamma-rays is $\Phi_\gamma = 1.237461 \times 10^{-14} \gamma cm^{-2} s^{-1}$. It is much lower than that of MAXI J1820+070 for every value of its α_* because of the larger inclination and the greater distance to Earth of XTE J1550-564.

5.3. XTE J1859+226

XTE J1859+226 is a BHXRB candidate at a distance $d = 4.8 - 5.8$ kpc [62] from Earth, so we adopt the value $d = 5.4$ kpc. Its donor star is a K-type [63], and we will assume that it is a main sequence star, so it will have an effective temperature $T_d = 3930$ K and a luminosity $L_{star} = 0.079 L_\odot$ [48]. The jet's Lorentz factor is in the region $\Gamma_b = 2 - 3$ [62], from which we obtain a bulk velocity $u_b = (0.87 - 0.94)c$, so we will adopt a value at the middle $u_b = 0.90c$. The jet half-opening angle is not measured, so we assume it to be $\xi = 1^\circ$. The spin of the black hole is calculated only by the RPM, which provides $\alpha_* = 0.149 \pm 0.005$ (1σ) [64]. The parameters that we use for XTE J1859+226 are depicted in Table 3.

Table 3. Main parameters of the BHXRB system XTE J1859+226.

XTE J1859+226				
$M_{BH}(M_\odot)$	$M_{donor}(M_\odot)$	d (kpc)	i (°)	P_{orb} (days)
7.8 [65]	0.55 [65]	5.4	66.6 [65]	0.276 [65]
$L_{star}(L_\odot)$	T_{eff} (K)	$u_b(c)$	ξ (°)	a_*
0.079	3930	0.90	1	0.149

Figure 4a depicts the proton distribution. It has similar values to the proton distribution of MAXI J1820+070 because the parameters of the two systems are similar. In Figure 4b, we see the intensity of neutrinos. It is similar to the one of MAXI J1820+070. The integral flux of neutrinos is $\Phi_\nu = 1.924216 \times 10^{-16} \nu \mathrm{cm}^{-2} \mathrm{s}^{-1}$. It is lower than that of MAXI J1820+070 because of the greater distance from Earth.

The attenuation of the accretion disk is depicted in Figure 4c. The attenuation is just a bit larger than MAXI J1820+070 for its case of $\alpha_* = 0.14$. This is because the two systems have similar parameters.

In Figure 4d, we see the intensity of high-energy gamma-rays. The intensity of gamma-rays is similar to that of MAXI J1820+070 due to the similar parameters of the two systems. The integral flux of high-energy gamma-rays is $\Phi_\gamma = 3.353376 \times 10^{-13} \gamma \mathrm{cm}^{-2} \mathrm{s}^{-1}$. It is a bit lower than that of MAXI J1820+070 for the case $\alpha_* = 0.14$ because of its greater distance to Earth.

It is worth noting that the results obtained for the three systems could change as time passes, as has already been foreshadowed by Equation (16). This can happen because the jets evolve over time and change the state that they are in; therefore, the parameters used above could vary over time, such as the jet's kinetic luminosity L_k, providing different results.

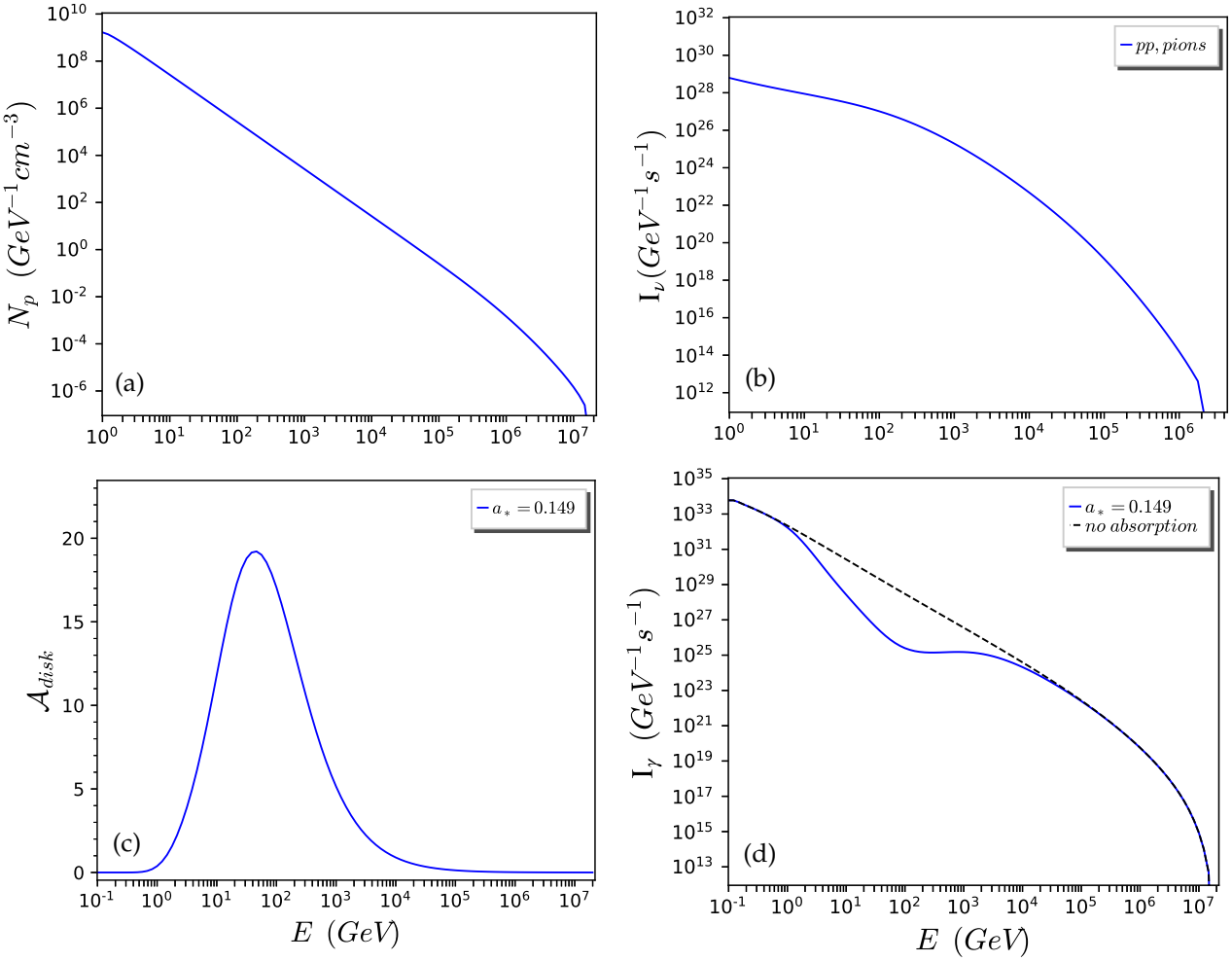

Figure 4. Results for XTE J1859+226: (**a**) proton distribution (N_p), (**b**) intensity of neutrinos (I_ν) by pion decay produced by p–p reactions, (**c**) accretion disk's attenuation ($\mathcal{A}_{disk}$), and (**d**) intensity of high-energy γ-rays (I_γ).

6. A New Technique for Measuring the Black Hole's Spin

In this work, in order to produce our results, we used values for the various parameters needed that have been proposed in recent research. The most important parameter for us is the dimensionless spin parameter α_*, representing the angular momentum of the black hole, which rotates around its axis.

For the measurement of α_*, there are three leading techniques, namely the continuum fitting method (CFM) [44], the X-ray reflection spectroscopy method (XRS) [45], and the relativistic precession model (RPM) [46]. These methods depend on the emitted (or reflected) X-ray spectrum from the accretion disk of the black hole. Each one is based on a theoretical model of the system. By altering the parameters of the system, they examine which set of these parameters the calculated theoretical X-ray spectrum fits the observed X-Ray spectrum best; thus, they lead to values of the parameters which are considered to be real under some uncertainties. For us, the important one from this set of parameters is the α_*.

The three methods that we described measure the black hole's spin by analyzing the X-ray spectrum of the accretion disk. However, the lepto-hadronic model deals with another part of the electromagnetic spectrum, the high-energy γ-ray spectrum, which is produced by the black hole's jets. By following the same methodology as the other three methods to carry out a fitting analysis on the observed high-energy γ-ray spectrum by performing calculations with the lepto-hadronic model for various sets of the parameters of

the system, we could extract a set of parameters that fits best the observations. In this way, this model could be used as a method for calculating the black hole's dimensionless spin parameter α_* that could complement the other three methods and, thus, determine which value is the real one. However, currently, there are only a few observations of high-energy γ-rays, which means that in order to measure the spin by our proposed technique, we should wait for appropriate observations, which we expect to have in the future.

Regarding the comparison of our proposed technique with the other three existing ones, the difference lies in the number of free parameters, since in the lepto-hadronic model, the number of free parameters is larger when compared to the models used by the other methods. However, the free parameters of the lepto-hadronic model are not completely "free". Estimates and ranges of these parameters have been proposed so they could be restricted by an appropriate distribution. Nevertheless, a detailed analysis should be carried out in order to validate the accuracy of our proposed method.

While there are no current observations of high-energy γ-rays for the studied systems, there are observations of soft γ-rays and X-rays. With our proposed technique, we could carry out a fitting analysis of these observations with predictions of soft γ-rays and X-rays. Such predictions have been made with photons produced by IC scattering and synchrotron radiation for the system of Cygnus X-1 [66]. Application to the studied systems of MAXI J1820+070, XTE J1550-564, and XTE J1859+226 is planned in future works.

7. Conclusions

In this work, we addressed the black hole's spin effects on the high-energy neutrino and γ-ray jet emissions from black hole X-ray binary systems (BHXRBs). Starting from the presentation of the accretion disk's properties, we specifically focused on the accretion disk's inner radius R_{in} and the accretion disk's temperature profile $T(R)$. Next, we paid special attention to the relativistic jets, the main reactions occurring inside them leading to neutrino and γ-ray production, and the transfer equation, which describes the energy distribution of each kind of particle. Subsequently, we computed the intensities and integral fluxes of high-energy neutrinos and γ-rays predicted by the lepto-hadronic model employed. Lastly, we explained the γ-rays' absorption mechanisms due to e^--e^+ pair production; in particular, absorption from the accretion disk's black-body emission.

By carrying out calculations for three BHXRB systems, MAXI J1820+070, XTE J1550-565, and XTE J1859+226, which have different spins (α_*), we investigated the effect of the black hole's spin on the expected spectra of high-energy neutrinos and γ-rays. From these calculations, we extracted the following conclusions:

1. The black hole's spin has no effect on the spectra of neutrino emissions. The intensity and the integral flux of the neutrinos remain the same for any value of α_*.
2. The black hole's spin has a strong effect on the spectra of high-energy γ-rays. The intensity and the integral flux of high-energy γ-rays decrease as the spin (α_*) increases. This happens because the accretion disk's attenuation, $\mathcal{A}_{disk}$, increases with α_*; therefore, a greater part of the γ-rays is annihilated.

As we have already implied, the lepto-hadronic model could be used as a method of measuring the spin α_* of the black hole of a BHXRB system by a fitting analysis of the predicted high-energy γ-ray spectra with the observed high-energy γ-ray spectra. Towards this purpose, appropriate observations of high-energy γ-rays from such systems are required. However, currently, such observational data are limited and there are not enough to carry out a fitting analysis of this kind. Despite this, next-generation telescopes (for example, ones using NASA's new gamma-ray detectors) may provide a rich amount of such measurements.

Author Contributions: Conceptualization, T.K. and O.K.; methodology, O.K.; software, O.K. and T.P.; validation, T.K. and O.K.; formal analysis, D.R. and T.P.; investigation, D.R. and T.P.; resources, O.K.; data curation, D.R.; writing—original draft preparation, D.R.; writing—review and editing, D.R., T.P., O.K. and T.K.; visualization, D.R.; supervision, T.K. and O.K.; project administration, T.K.

and O.K.; funding acquisition, O.K. All authors have read and agreed to the published version of the manuscript.

Funding: The authors T.P., O.K., and T.K. wish to acknowledge financial support from the Association for Advancement of Research on Open Problems (OPRA Association, Tel Aviv, Israel) in Nuclear Physics and Particle Physics, project No 83241/ELKE-UoI.

Data Availability Statement: The datasets generated during and/or analyzed in the present study are available upon request from the corresponding author.

Conflicts of Interest: Author Odysseas Kosmas was employed by the company Conigital Ltd. The remaining authors declare that the research was conducted in the absence of any commercial or financial relationships that could be construed as a potential conflict of interest.

Abbreviations

The following abbreviations are used in this manuscript:

BHXRB	Black Hole X-Ray Binary
R_{ISCO}	Radius of the Innermost Stable Circular Orbit

References

1. De Rosa, A.; Vignali, C.; Bogdanović, T.; Capelo, P.R.; Charisi, M.; Dotti, M.; Husemann, B.; Lusso, E.; Mayer, L.; Paragi, Z.; et al. The quest for dual and binary supermassive black holes: A multi-messenger view. *New Astron. Rev.* **2019**, *86*, 101525. [CrossRef]
2. Branchesi, M. Multi-messenger astronomy: Gravitational waves, neutrinos, photons, and cosmic rays. *J. Phys. Conf. Ser.* **2016**, *718*, 022004. [CrossRef]
3. Ferrigno, C.; Savchenko, V.; Coleiro, A.; Panessa, F.; Bazzano, A.; Bozzo, E.; Chenevez, J.; Domingo, A.; Doyle, M.; Goldwurm, A.; et al. Multi-messenger astronomy with INTEGRAL. *New Astron. Rev.* **2021**, *92*, 101595. [CrossRef]
4. Abbasi, R.; Abdou, Y.; Abu-Zayyad, T.; Ackermann, M.; Adams, J.; Aguilar, J.; Ahlers, M.; Allen, M.; Altmann, D.; Andeen, K.; et al. The design and performance of IceCube DeepCore. *Astropart. Phys.* **2012**, *35*, 615–624. [CrossRef]
5. Aartsen, M.G.; Abbasi, R.; Ackermann, M.; Adams, J.; Aguilar, J.A.; Ahlers, M.; Ahrens, M.; Alispach, C.; Allison, P.; Amin, N.M.; et al. IceCube-Gen2: The window to the extreme Universe. *J. Phys. G Nucl. Part. Phys.* **2021**, *48*, 060501. [CrossRef]
6. Padovani, P.; Alexander, D.M.; Assef, R.J.; De Marco, B.; Giommi, P.; Hickox, R.C.; Richards, G.T.; Smolčić, V.; Hatziminaoglou, E.; Mainieri, V.; et al. Active galactic nuclei: What's in a name? *Astron. Astrophys. Rev.* **2017**, *25*, 2. [CrossRef]
7. Murase, K. Active Galactic Nuclei as High-Energy Neutrino Sources. In *Neutrino Astronomy: Current Status, Future Prospects*; World Scientific Publishing Co. Pte. Ltd.: Singapore; 2017; pp. 15–31.
8. Pagliaroli, G.; Villante, F.L. A multi-messenger study of the total galactic high-energy neutrino emission. *J. Cosmol. Astropart. Phys.* **2018**, *2018*, 035. [CrossRef]
9. Kantzas, D.; Markoff, S.; Lucchini, M.; Ceccobello, C. Black-hole X-ray binaries in the new era of multi-messenger Astronomy. *PoS* **2021**, *ICRC2021*, 1011.
10. Shidatsu, M.; Nakahira, S.; Murata, K.L.; Adachi, R.; Kawai, N.; Ueda, Y.; Negoro, H. X-ray and optical monitoring of state transitions in MAXI J1820+ 070. *Astrophys. J.* **2019**, *874*, 183. [CrossRef]
11. Rodi, J.; Tramacere, A.; Onori, F.; Bruni, G.; Sànchez-Fernàndez, C.; Fiocchi, M.; Natalucci, L.; Ubertini, P. A broadband view on microquasar MAXI J1820+ 070 during the 2018 outburst. *Astrophys. J.* **2021**, *910*, 21. [CrossRef]
12. Chaty, S.; Dubus, G.; Raichoor, A. Near-infrared jet emission in the microquasar XTE J1550-564. *Astron. Astrophys.* **2011**, *529*, A3. [CrossRef]
13. Sriram, K.; Rao, A.R.; Choi, C.S. Study of a Sudden QPO Transition Event in the Black Hole Source XTE J1550-564. *Astrophys. J.* **2016**, *823*, 67.
14. Bellm, E.C.; Wang, Y.; van Roestel, J.; Phillipson, R.A.; Coughlin, M.W.; Tomsick, J.A.; Groom, S.L.; Healy, B.; Purdum, J.; Rusholme, B.; et al. An Optically Discovered Outburst from XTE J1859+ 226. *Astrophys. J.* **2023**, *956*, 21. [CrossRef]
15. Farinelli, R.; Amati, L.; Shaposhnikov, N.; Frontera, F.; Masetti, N.; Palazzi, E.; Landi, R.; Lombardi, C.; Orlandini, M.; Brocksopp, C. Spectral evolution of the X-ray nova XTE J1859+ 226 during its outburst observed by BeppoSAX and RXTE. *Mon. Not. R. Astron. Soc.* **2013**, *428*, 3295–3305. [CrossRef]
16. Romero, G.E.; Torres, D.F.; Kaufman Bernadó, M.M.; Mirabel, I.F. Hadronic gamma-ray emission from windy microquasars. *Astron. Astrophys.* **2003**, *410*, L1–L4. [CrossRef]
17. Papavasileiou, T.; Kosmas, O.; Sinatkas, I. Simulations of Neutrino and Gamma-Ray Production from Relativistic Black-Hole Microquasar Jets. *Galaxies* **2021**, *9*, 67. [CrossRef]
18. Papavasileiou, T.; Kosmas, O.; Sinatkas, I. Relativistic Magnetized Astrophysical Plasma Outflows in Black-Hole Microquasars. *Symmetry* **2022**, *14*, 485. [CrossRef]
19. Gould, R.J.; Schréder, G.P. Pair production in photon-photon collisions. *Phys. Rev.* **1967**, *155*, 1404.

20. Papavasileiou, T.V.; Kosmas, O.T.; Sinatkas, I. Prediction of gamma-ray emission from Cygnus X-1, SS 433, and GRS 1915+ 105 after absorption. *Astron. Astrophys.* **2023**, *673*, A162.
21. Papavasileiou, T.; Kosmas, O.; Sinatkas, I. Studying the Spectral Energy Distributions Emanating from Regular Galactic XRBs. *Universe* **2023**, *9*, 312. [CrossRef]
22. Kosmas, O.; Papavasileiou, T.; Kosmas, T. Integral Fluxes of Neutrinos and Gamma-Rays Emitted from Neighboring X-ray Binaries. *Universe* **2023**, *9*, 517. [CrossRef]
23. Shakura, N.I.; Sunyaev R.S. Black holes in binary systems. Observational appearance. *Astron. Astrophys.* **1973**, *24*, 337–355.
24. Bardeen, J.M.; Press, W.H.; Teukolsky, S.A. Rotating black holes: Locally nonrotating frames, energy extraction, and scalar synchrotron radiation. *Astrophys. J.* **1972**, *178*, 347–370. [CrossRef]
25. Frank, J.; King, A.; Raine, D. *Accretion Power in Astrophysics*, 3rd ed.; Cambridge University Press: Cambridge, UK, 2002.
26. Mukhopadhyay, B. Description of pseudo-Newtonian potential for the relativistic accretion disks around Kerr black holes. *Astrophys. J.* **2002**, *581*, 427. [CrossRef]
27. Rarras, D.; Kosmas, T.; Papavasileiou, T.; Kosmas, O. Galactic Stellar Black Hole Binaries: Spin Effects on Jet Emissions of High-Energy Gamma-Rays. *Particles* **2024**, *7*, 792–804. [CrossRef]
28. Böttcher, M.; Dermer, C.D. Photon-Photon Absorption of Very High Energy Gamma Rays from Microquasars: Application to LS 5039. *Astrophys. J.* **2005**, *634*, L81–L84. [CrossRef]
29. Cerutti, B.; Dubus, G.; Malzac, J.; Szostek, A.; Belmont, R.; Zdziarski, A.A.; Henri, G. Absorption of high-energy gamma rays in Cygnus X-3. *Astron. Astrophys.* **2011**, *529*, A120. [CrossRef]
30. Romero, G.E.; Vila, G.S. The proton low-mass microquasar: High-energy emission. *Astron. Astrophys.* **2008**, *485*, 623–631. [CrossRef]
31. Mannheim, K.; Schlickeiser, R. Interactions of cosmic ray nuclei. *Astron. Astrophys.* **1994**, *286*, 983–996.
32. Papadopoulos, D.A.; Kosmas, O.T.; Ganatsios, S. Modeling Particle Transport in Astrophysical Outflows and Simulations of Associated Emissions from Hadronic Microquasar Jets. *Adv. High Energy Phys.* **2022**, *2022*, 8146675 [CrossRef]
33. Smponias, T.; Kosmas, O.T. Neutrino Emission from Magnetized Microquasar Jets. *Adv. High Energy Phys.* **2017**, *2017*, 4962741. [CrossRef]
34. Zhang, J.F.; Li, Z.R.; Xiang, F.Y.; Lu, J.F. Electron transport with re-acceleration and radiation in the jets of X-ray binaries. *Mon. Not. R. Astron. Soc.* **2017**, *473*, 3211–3222. [CrossRef]
35. Kosmas, O.T.; Leyendecker, S. Phase lag analysis of variational integrators using interpolation techniques *PAMM Proc. Appl. Math. Mech.* **2012**, *12*, 677–678.
36. Kosmas, O.T.; Leyendecker, S. Family of high order exponential variational integrators for split potential systems. *J. Phys. Conf. Ser.* **2015**, *574*, 012002. [CrossRef]
37. Kosmas, O.T.; Vlachos, D.S. A space-time geodesic approach for phase fitted variational integrators. *Phys. Conf. Ser.* **2016**, *738*, 012133. [CrossRef]
38. Reynoso, M.M.; Romero, G.E.; Christiansen, H.R. Production of gamma rays and neutrinos in the dark jets of the microquasar SS433. *Mon. Not. R. Astron. Soc.* **2008**, *387*, 1745–1754. [CrossRef]
39. Reynoso, M.M.; Romero, G.E. Magnetic field effects on neutrino production in microquasars. *Astron. Astrophys.* **2009**, *493*, 1–111. [CrossRef]
40. Kantzas, D.; Markoff, S.; Beuchert, T.; Lucchini, M.; Chhotray, A.; Ceccobello, C.; Tetarenko, A.J.; Miller-Jones, J.C.A.; Bremer, M.; Garcia, J.A.; et al. A new lepto-hadronic model applied to the first simultaneous multiwavelength data set for Cygnus X–1. *Mon. Not. R. Astron. Soc.* **2021**, *500*, 2112–2126. [CrossRef]
41. Carulli, A.M.; Reynoso, M.M; Romero, G.E. Neutrino production in Population III microquasars. *Astropart. Phys.* **2021**, *128*, 102557. [CrossRef]
42. Stern, B.E.; Poutanen, J. Gamma-ray bursts from synchrotron self-Compton emission. *Mon. Not. R. Astron. Soc.* **2004**, *352*, L35–L39. [CrossRef]
43. Jones, F.C. Calculated spectrum of inverse-Compton-scattered photons. *Phys. Rev.* **1968**, *167*, 1159. [CrossRef]
44. McClintock, J.E.; Narayan, R.; Steiner, J.F. Black hole spin via continuum fitting and the role of spin in powering transient jets. In *The Physics of Accretion onto Black Holes*; Springer: Berlin/Heidelberg, Germany, 2015; pp. 295–322.
45. Reynolds, C.S. Measuring black hole spin using X-ray reflection spectroscopy. In *The Physics of Accretion onto Black Holes* ; Springer: Berlin/Heidelberg, Germany, 2015; pp. 277–294.
46. Ingram, A.; Motta, S. Solutions to the relativistic precession model. *Mon. Not. R. Astron. Soc.* **2014**, *444*, 2065–2070. [CrossRef]
47. Mikołajewska, J.; Zdziarski, A.A.; Ziółkowski, J.; Torres, M.A.P.; Casares, J. The Donor of the Black Hole X-Ray Binary MAXI J1820+ 070. *Astrophys. J.* **2022**, *930*, 9. [CrossRef]
48. Mignard, F. Astronomical distance scales. *Comptes Rendus Phys.* **2019**, *20*, 140–152. [CrossRef]
49. Zhao, X.; Gou, L.; Dong, Y.; Tuo, Y.; Liao, Z.; Li, Y.; Jia, N.; Feng, Y.; Steiner, J.F. Estimating the black hole spin for the X-ray binary MAXI J1820+ 070. *Astrophys. J.* **2021**, *916*, 108. [CrossRef]
50. Draghis, P.A.; Miller, J.M.; Zoghbi, A.; Reynolds, M.; Costantini, E.; Gallo, L.C.; Tomsick, J.A. A systematic view of ten new black hole spins. *Astrophys. J.* **2023**, *945*, 19. [CrossRef]
51. Bhargava, Y.; Belloni, T.; Bhattacharya, D.; Motta, S.; Ponti, G. A timing-based estimate of the spin of the black hole in MAXI J1820+ 070. *Mon. Not. R. Astron. Soc.* **2021**, *508*, 3104–3110. [CrossRef]

52. Poutanen, J.; Veledina, A.; Berdyugin, A.V.; Berdyugina, S.V.; Jermak, H.; Jonker, P.G.; Kajava, J.J.E.; Kosenkov, I.A.; Kravtsov, V.; Piirola, V.; et al. Black hole spin–orbit misalignment in the x-ray binary MAXI J1820+ 070. *Science* **2022**, *375*, 874–876. [CrossRef]
53. Kalogera, V. Spin-orbit misalignment in close binaries with two compact objects. *Astrophys. J.* **2000**, *541*, 319. [CrossRef]
54. Torres, M.A.P.; Casares, J.; Jiménez-Ibarra, F.; Álvarez-Hernández, A.; Muñoz-Darias, T.; Padilla, M.A.; Jonker, P.G.; Heida, M. The binary mass ratio in the black hole transient MAXI J1820+ 070. *Astrophys. J. Lett.* **2020**, *893*, L37. [CrossRef]
55. Atri, P.; Miller-Jones, J.C.A.; Bahramian, A.; Plotkin, R.M.; Deller, A.T.; Jonker, P.G.; Maccarone, T.J.; Sivakoff, G.R.; Soria, R.; Altamirano, D.; et al. A radio parallax to the black hole X-ray binary MAXI J1820+ 070. *Mon. Not. R. Astron. Soc. Lett.* **2020**, *493*, L81–L86. [CrossRef]
56. Zdziarski, A.A.; Tetarenko, A.J., Sikora, M. Jet Parameters in the Black Hole X-Ray Binary MAXI J1820+ 070. *Astrophys. J.* **2022**, *925*, 189. [CrossRef]
57. Orosz, J.A.; Steiner, J.F.; McClintock, J.E.; Torres, M.A.P.; Remillard, R.A.; Bailyn, C.D.; Miller, J.M. An improved dynamical model for the microquasar XTE J1550- 564. *Astrophys. J.* **2011**, *730*, 75. [CrossRef]
58. Miller-Jones, J.C.A.; Fender, R.P.; Nakar, E. Opening angles, Lorentz factors and confinement of X-ray binary jets. *Mon. Not. R. Astron. Soc.* **2006**, *367*, 1432–1440. [CrossRef]
59. Kaaret, P.; Corbel, S.; Tomsick, J.A.; Fender, R.; Miller, J.M.; Orosz, J.A.; Tzioumis, A.K.; Wijnands, R. X-Ray Emission from the Jets of XTE J1550–564. *Astrophys. J.* **2003**, *582*, 945. [CrossRef]
60. Steiner, J.F.; Reis, R.C.; McClintock, J.E.; Narayan, R.; Remillard, R.A.; Orosz, J.A.; Gou, L.; Fabian, A.C.; Torres, M.A.P. The spin of the black hole microquasar XTE J1550- 564 via the continuum-fitting and Fe-line methods. *Mon. Not. R. Astron. Soc.* **2011**, *416*, 941–958. [CrossRef]
61. Motta, S.E.; Muñoz-Darias, T.; Sanna, A.; Fender, R.; Belloni, T.; Stella, L. Black hole spin measurements through the relativistic precession model: XTE J1550-564. *Mon. Not. R. Astron. Soc. Lett.* **2014**, *439*, L56–L69. [CrossRef]
62. Nandi, A.; Mandal, S.; Sreehari, H.; Radhika, D.; Das, S.; Chattopadhyay, I.; Iyer, N.; Agrawal, V.K.; Aktar, R. Accretion flow dynamics during 1999 outburst of XTE J1859+ 226-modeling of broadband spectra and constraining the source mass. *Astrophys. Space Sci.* **2018**, *363*, 90. [CrossRef]
63. Kimura, M.; Done, C. Evolution of X-ray irradiation during the 1999–2000 outburst of the black hole binary XTE J1859+ 226. *Mon. Not. R. Astron. Soc.* **2019**, *482*, 626–638. [CrossRef]
64. Motta, S.E.; Belloni, T.; Stella, L.; Pappas, G.; Casares, J.; Muñoz-Darias, A.T.; Torres, M.A.P.; Yanes-Rizo, I.V. Black hole mass and spin measurements through the relativistic precession model: XTE J1859+ 226. *Mon. Not. R. Astron. Soc.* **2022**, *517*, 1469–1475. [CrossRef]
65. Yanes-Rizo, I.V.; Torres, M.A.P.; Casares, J.; E Motta, S.; Muñoz-Darias, T.; Rodríguez-Gil, P.; Padilla, M.A.; Jiménez-Ibarra, F.; Jonker, P.G.; Corral-Santana, J.M.; et al. A refined dynamical mass for the black hole in the X-ray transient XTE J1859+ 226. *Mon. Not. R. Astron. Soc.* **2022**, *517*, 1476–1482. [CrossRef]
66. Papavasileiou, T.V.; Kosmas, O.; Kosmas, T.S. A direct method for reproducing fully relativistic spectra from standard accretion disks by modifying their inner boundary. *arXiv* **2024**, arXiv:2408.02415.

Disclaimer/Publisher's Note: The statements, opinions and data contained in all publications are solely those of the individual author(s) and contributor(s) and not of MDPI and/or the editor(s). MDPI and/or the editor(s) disclaim responsibility for any injury to people or property resulting from any ideas, methods, instructions or products referred to in the content.